Appl. Phys. B 78, 781–790 (2004)
DOI: 10.1007/s00340-004-1488-4

Applied Physics B
Lasers and Optics

N. CAO[1,2]
Y.K. HO[1,✉]
Y.J. XIE[1]
J. PANG[1]
Z. CHEN[1]
L. SHAO[1]
Q. KONG[1]
Q.S. WANG[2]

Interaction of an electron bunch with a laser pulse in vacuum

[1] Institute of Modern Physics, Fudan University, Shanghai 200433, P.R. China
[2] North-West Institute of Nuclear Technology, Xi'an 710024, P.R. China

Received: 20 January 2003/
Revised version: 13 November 2003
Published online: 7 April 2004 •

ABSTRACT The output properties of electrons accelerated by the vacuum laser acceleration scheme CAS (capture and acceleration scenario) are addressed. The transport process of the electron bunch, the fraction of the CAS electrons of the incident electrons, the correlation of electron energy with position and scattering angle, the energy spectrum and angular distributions as well as the emittance of the outgoing electrons are studied at a laser intensity of $a_0 = 10$. In addition, the effects of the laser intensity, beam width, and pulse duration on the properties of the output electrons are also examined. Physical explanations of those output characteristics are presented based on the mechanism behind the CAS scheme. The feasibility of CAS to become a realistic laser accelerator scheme is explored.

PACS 41.75.Jv; 42.60.Jf; 41.85.Ja

1 Introduction

Ever since the emergence of the first accelerator in England, the accelerator beam energy has been increased about ten times every ten years [1]. With the increasing demand of even higher energies in particle physics and other areas, the building expense and complexity of accelerators also have risen drastically, and scientists have had to explore new acceleration mechanisms for decades. Laser acceleration of charged particles has been actively researched [2]. The far-field laser acceleration of free electrons in vacuum has attracted much attention because it avoids some of the difficulties associated with laser-driven acceleration in plasma [3–5]. Recently it was shown, via experiment [3] and simulation [4], that low-energy electrons interacting with a focused laser pulse could be ponderomotively scattered and receive net energy gains from the field by the nonlinear ponderomotive laser force, but the energy gain is intrinsically limited to relatively low values, i.e., less than 10 MeV for presently obtainable laser intensities [4]. In contrast, based on a novel vacuum laser acceleration scheme, i.e., the capture and acceleration scenario (CAS) [5], the energy gain is found to be greater than 100 MeV for present day lasers ($a_0 \approx 10$) and even exceeds GeV in the regime of ultra-high intensities of $a_0 \gtrsim 100$. Here $a_0 = eE_0/(m_e\omega c) = 8.5 \times 10^{-10}(\lambda I^{1/2})$ with λ the laser wavelength in μm, I the intensity in W/cm^2, E_0 the electric field amplitude of the laser beam at focus, ω the laser frequency, e, m_e the electron charge and mass, respectively, and c the speed of light in vacuum [5].

According to the Lawson–Woodward theorem [6], a light beam in the far-field is the superposition of plane waves propagating in different directions, thus its effect on a particle is the sum of the plane wave effects. Since a particle moves at velocity less than c and a plane wave moves at c in vacuum, the particle must slip relative to the phase of the wave. Because of the phase slippage, the effect of light on a particle averages to zero if the interaction is unbounded. This theory assumed that (i) the electron trajectory is a straight line with a speed v_e approximately equal to the speed of light in vacuum, $v_e \approx c$, which is unperturbed by the laser field, and (ii) the interaction region is infinite in extent.

Simulations [5] indicated that, in the regime of CAS, the electron trajectory is significantly perturbed by the laser field as it enters the high- intensity channel, which in effect limits the interaction region, thereby circumventing the Lawson–Woodward theorem. Hence, large energy gains are obtained without limiting the interaction distance by the use of additional optics (as required in [7]).

The physical mechanism behind CAS is the following. For a focused laser beam propagating in vacuum, there exists a subluminous wave phase velocity region. This region of lower phase velocity occurs off the axis at a radius comparable to the local radius of the laser beam and extends a few Rayleigh lengths along the beam axis. In conjunction with the strong longitudinal electric field component, which is the chief acceleration field, this region forms an acceleration channel that shows similar characteristics to that of a wave guide tube of conventional accelerators. Relativistic electrons injected into this acceleration channel can be trapped and remain in an acceleration phase of the laser field for a sufficiently long time, thereby obtaining considerable energy from the field. The basic conditions for CAS to occur have been found as follows. (i) The laser intensity should be very strong, $a_0 \gtrsim 5$. (ii) The electron injection energy should be

✉ Fax: +86-21/6564-3815, E-mail: hoyk@fudan.ac.cn

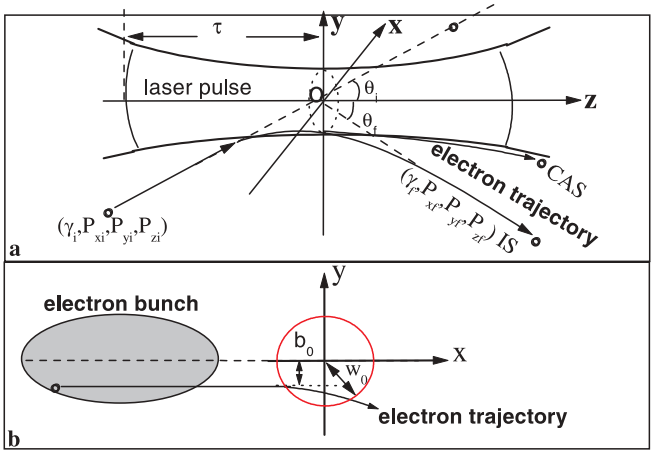

FIGURE 1 **a** Schematic geometry of electron scattering by a laser beam. The laser propagates along the z-axis, w_0 is the beam width at the waist, τ is the laser pulse duration. Without loss of generality, we assume that the electrons are coming in from the negative-x side parallel to the x–z plane. (γ_i, p_{xi}, p_{yi}, p_{zi}) and (γ_f, p_{xf}, p_{yf}, p_{zf}) denote the initial and final state of an electron, p is the electron momentum, γ is the Lorentz factor and b_0 the impact parameter. The electron injection angle with respect to the laser beam is $\theta = \tan^{-1}(p_{xi}/p_{zi})$. **b** The right side view of **a**

in the range 5–15 MeV. (iii) The electron incident crossing angle (relative to the beam direction) should be small, typically $\tan\theta \approx 0.1$–0.15 (see Fig. 1). The resulting energy gain is found to be in agreement with theoretical estimates of the acceleration by the axial electric field.

According to the theory of Quantum Electrodynamics, there are three fundamentally different energy-exchange mechanisms between free electrons and laser fields in vacuum, namely normal Compton scattering (NCS); stimulated Compton scattering (SCS); and non-linear Compton scattering (NLCS). NLCS is a multi-photon exchange process where an electron absorbs simultaneously many photons with emission of one high-frequency photon. These three mechanisms play a different role in the laser acceleration of electrons at different laser intensity. For laser acceleration, the contribution of NCS can be neglected because the energy of a photon is of the order of a few eV. Federov et al. [8] pointed out that SCS leads to electron inelastic scattering by laser beams, which can be classically described by the ponderomotive potential model. We proposed [5] that the principal contribution to vacuum laser acceleration (tremendous energy exchange) comes from the NLCS process. However, this is still an open problem, and we plan to study this problem in the future.

Most of the previous studies are based on the single-electron model. For a realistic case, an electron bunch has to be considered. Also, to study CAS as a potential accelerator scheme, one has to examine the output properties of the accelerated electrons. The features of the interaction process, the properties of the energy and angular spectra, and emittance of the output electrons, etc., as well as the influence of the laser parameters etc., have to be studied in more detail. These are the main objectives of this paper.

It is organized as follows. The theoretical model is given in Sect. 2. In Sect. 3, the physics underlying the CAS scheme is presented. In Sect. 4, numerical simulations of the output properties of the CAS electrons are described and discussed. Section 5 is a brief summary.

2 Theoretical model

In order to satisfy the classical description of radiation and electron motion in the electromagnetic field [9], the electron de Broglie wavelength must be much less than the characteristic wave length of the system and the effect of quantum recoil must be small. This can be expressed as

$$\frac{\gamma m_e c^2 \beta}{eE_0} \gg \frac{\hbar}{\gamma m_e c}\,, \quad \gamma m_e c^2 \gg \frac{\hbar\gamma^2 e E_0}{m_e c}\,. \tag{1}$$

For the relativistic case, the above relations can be reduced to

$$\sqrt{\frac{E_0}{E_c}} = \sqrt{\frac{a_0\hbar\omega}{m_e c^2}} \ll \gamma \ll \frac{E_c}{E_0} = \frac{m_e c^2}{a_0\hbar\omega}\,, \tag{2}$$

where $E_c = m_e^2 c^3/(e\hbar) \approx 1.3\times 10^{16}\,\mathrm{V/cm}$ is the so-called critical field strength for the production of an electron-positron pair, E_0 is the peak amplitude of the laser field, $\beta = v/c$, and γ is the Lorentz factor representing the electron energy. The maximum field strength $E_0(\mathrm{V/cm}) = 3.21\times 10^{10}\, a_0/\lambda\ (\mu\mathrm{m})$ used in the examples of this paper is $E_0 = 2.6\times 10^{12}\,\mathrm{V/cm} \ll E_c$ for $a_0 = 80$ and $\lambda = 1\,\mu\mathrm{m}$. Relation (2) is satisfied in all cases considered. Hence, a classical description of the radiation field and electron is adequate.

In our calculations, a single, linearly polarized laser pulse is considered. Figure 1 gives the schematics of the electron-laser interaction.

A prolate ellipsoid electron bunch is injected into the laser field with its central section including the major axis being in the x–z plane. Without loss of generality, we assume that, under the condition of electrons moving freely, i.e., without the influence of the laser field, the center of the pulsed laser beam and that of the injected electron bunch reach the point $x = y = z = 0$ synchronously at $t = 0$.

For a laser beam of Hermite–Gaussian $(0, 0)$ mode polarized in the x-direction and propagating along the z-axis, the transverse electric field component can be expressed as [5, 10, 11]

$$\begin{aligned} E_x(x,y,z,t) = E_0\frac{w_0}{w(z)}\exp\left(-\frac{x^2+y^2}{w(z)^2}\right) \\ \times\exp\left[\mathrm{i}\left(kz-\omega t-\tan^{-1}\left(\frac{2z}{kw_0^2}\right)\right.\right. \\ \left.\left.-\varphi_0+\frac{k\left(x^2+y^2\right)}{2R(z)}\right)\right]\times f(ct-z)\,, \end{aligned} \tag{3}$$

where E_0 is the on-axis electric-field strength in the focal plane $z = 0$, w_0 is the beam waist, φ_0 is the initial phase, and k is the laser wave number. The remaining quantities are defined through the equations

$$w(z) = w_0\left[1+\left(\frac{2z}{kw_0^2}\right)^2\right]^{\frac{1}{2}}\,, \tag{4}$$

$$R(z) = z\left[1+\left(\frac{kw_0^2}{2z}\right)^2\right]\,, \tag{5}$$

$$f(ct-z) = \exp\left(-\frac{(t-\frac{z}{c})^2}{\tau^2}\right)\,, \tag{6}$$

where $w(z)$ is the beam radius, $R(z)$ is the curvature radius of the wave front, f is the electric field envelope, and τ is the pulse duration. To study the detailed dynamics of electrons in the laser field, three dimensional test particle simulations are utilized to solve the relativistic Newton–Lorentz equation of motion

$$\frac{\mathrm{d}\boldsymbol{P}}{\mathrm{d}t} = -e(\boldsymbol{E} + \boldsymbol{V} \times \boldsymbol{B}) \,, \tag{7}$$

where $\boldsymbol{P} = \gamma m V$ is the electron momentum, $\boldsymbol{v}$ is the electron velocity in units of c, and $\boldsymbol{E}$ and $\boldsymbol{B}$ are the electric and magnetic fields of the laser pulse, respectively. To solve the equation of motion, in addition to E_x given by (3), the other electric and magnetic field components are obtained from [12]

$$E_z = (\mathrm{i}/k)(\partial E_x/\partial x) \,, \tag{8}$$

$$\boldsymbol{B} = -(\mathrm{i}/\omega)\nabla \times \boldsymbol{E} \,. \tag{9}$$

The electromagnetic field given here is the analytical expression in the paraxial approximation for pulsed Gaussian beams. According to the discussions of Barton [13], the fifth-order corrected field equations are of high accuracy. Our study shows that the paraxial approximation [14] is a better description than the lowest-order and the third-order correction as it includes some higher-order terms in its magnetic components; for electron dynamics in an intense laser field, the paraxial approximation model is applicable for $kw \gtrsim 50$. When the beam waist is in the range of $40 \lesssim kw_0 < 50$, the paraxial field is no longer useful, and the fifth-order corrected model is needed. For $kw_0 \lesssim 30$, it seems that the seventh-order corrected model or even higher orders are needed. Thus, in this article, for the parameters used here, the effect of the higher-order corrections can be ignored, and we adopt the paraxial approximation model. The equation of motion (7) is solved by using the fourth-order Runge–Kutta method together with Richardson's first-order extrapolation procedure.

A four-dimensional energy-momentum configuration is used to specify the electron state as (γ, p_x, p_y, p_z), where γ is the Lorentz factor and the momentum, p, is normalized in the units of $m_e c$; $(\gamma_i, p_{xi}, p_{yi}, p_{zi})$ denotes the initial state and $(\gamma_f, p_{xf}, p_{yf}, p_{zf})$ the final state after the interaction. For simplicity, throughout this letter, time and length are normalized by $1/\omega$ and $1/k$, respectively. The electron injection angle with respect to the z axis is $\theta = \tan^{-1}(p_{xi}/p_{zi})$.

In studying the interaction of electrons with laser pulses, one may raise questions about space charge effects caused by the surrounding electrons in the bunch and the retardant force induced by the radiation effect. Our studies [5] show that, compared with the external force caused by the intensive laser field, these two effects can be neglected in the cases considered here.

3 The physics underlying the CAS scheme [5]

For a laser beam of Hermite–Gaussian (0, 0) mode polarized in the x-direction and propagating along the z-axis, the phase of the laser field is

$$\varphi = kz - \omega t - \tan^{-1}\alpha + \frac{kr^2}{2z(1+1/\alpha^2)} \,, \tag{10}$$

where $\alpha = z/Z_\mathrm{R}$, $Z_\mathrm{R} = kw_0^2/2$ is the Rayleigh length, and $r^2 = x^2 + y^2$. The effective phase velocity of the wave along a particle trajectory, $(v_\varphi)_J$, can be calculated using the equation

$$\partial\varphi/\partial t + (v_\varphi)_J(\nabla\varphi)_J = 0 \,, \tag{11}$$

where $(\nabla\varphi)_J$ is the gradient of the phase of the laser field. The effective phase velocity along a trajectory parallel to the z-axis is

$$v_{\varphi z} = ck/(\partial\varphi/\partial z) \,. \tag{12}$$

The minimum phase velocity occurs for $\boldsymbol{v}_\varphi \parallel \nabla\varphi$

$$v_{\varphi\mathrm{m}} = ck/|\nabla\varphi| \,. \tag{13}$$

The angle, θ_m, between $v_{\varphi\mathrm{m}}$ and the z-axis is, given by

$$\tan\theta_\mathrm{m} = \frac{\partial\varphi/\partial r}{\partial\varphi/\partial z} \,, \tag{14}$$

with

$$\partial\varphi/\partial z = k\left[1 - \frac{(1-f_\varphi)}{kZ_\mathrm{R}(1+\alpha^2)}\right] \,, \tag{15}$$

$$\partial\varphi/\partial r = \frac{kr\alpha}{Z_\mathrm{R}(1+\alpha^2)} \,, \quad \text{and} \tag{16}$$

$$f_\varphi = \frac{r^2(1-\alpha^2)}{w_0^2(1+\alpha^2)} \,. \tag{17}$$

From these equations, it is straightforward to find the subluminous phase velocity regions. The condition $v_{\varphi z} < c$ requires $f_\varphi > 1$, which can only occur in the region $z < Z_\mathrm{R}$. Moreover, at $z = 0$, $f_\varphi > 1$ occurs only for $r > w_0$. As for the minimum phase velocity, the condition $v_{\varphi\mathrm{m}} < c$ requires $r > w(z)$, and the magnitude and direction in the subluminous phase velocity region characterized by $0 < |Z| < Z_\mathrm{R}/3$ and $r \sim \sqrt{3/2}w_0$ is approximately $v_{\varphi\mathrm{m}} \sim c\left[1 - 1/(kw_0)^2\right]$ and $\theta_\mathrm{m} \sim 1/(kw_0)$ at $Z \sim Z_\mathrm{R}/3$.

Notice that the effective phase velocity along the z-axis is superluminous, $(v_{\varphi z})_{r=0} \sim c/\{1 - 1/[kZ_\mathrm{R}(1+\alpha^2)]\}$. This indicates that the phase velocity in the near-axis region of the beam is not suitable for accelerating charged particles since the high phase velocity ($v_{\varphi z} > c$) leads to fast phase slippage.

Phase velocity synchronization plays an important role in the CAS scheme. For an electron moving near the speed of light c in a straight line along the z-axis, the phase velocity of the laser field is greater than c. In this case, phase synchronization and hence, significant energy gain do not occur. However, an electron undergoing a curved trajectory passing through the lower phase velocity region, which is the case of the CAS trajectory, can move in phase with the laser field over a significant distance. This can lead to a substantial net energy gain.

For accelerating particles, in addition to the subluminous phase velocity, the field strength, the amplitude of the longitudinal electric field, is also an important factor. We therefore introduce a quantity Q that combines these two factors to represent the ability of the laser field for accelerating charged particles. We determine the acceleration quality factor

$$Q = Q_0(1 - V_{\varphi\mathrm{m}}/c)[x/w(z)]\exp[-(x^2+y^2)/w(z)^2] \,. \tag{18}$$

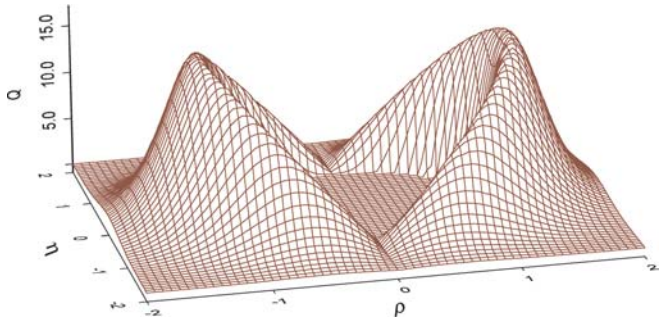

FIGURE 2 The acceleration quality factor Q versus $\varrho = x/w_0$ and $\eta = y/w_0$ in the $z = 0$ plane of a focused laser beam with $kw_0 = 60$

for $V_{\varphi m} \leq c$, and by $Q = 0$ for $V_{\varphi m} > c$. Here Q_0 is a normalization constant chosen to make Q of order of unity. In (18), $1 - V_{\varphi m}/c$ represents the contribution from the phase velocity and the remaining term is proportional to the amplitude of the longitudinal electric field, describing the effect of the laser intensity on the electron behavior. The distribution of the acceleration quality factor Q in the plane $z = 0$ for a focused laser beam with $kw_0 = 60$ is given in Fig. 2.

Significant values of Q emerge just beyond the beam width and are concentrated in the areas near the polarization plane. This is because the lower phase velocity region is located in the outer region of the beam and the large amplitudes of the axial electric field are distributed near the polarization plane ($y = 0$). This is the favorable region for accelerating electrons, and we call it the acceleration channel of the laser beam propagation in vacuum. It is also of interest to note that, in the region near the beam axis, Q equals 0 because $V_{\varphi m} > c$ there. The region near the beam axis is not suited for accelerating charged particles, because there the phase velocity is highest and the amplitude of the axial electric field is small. Along the diffraction angle ($\sim 1/kw_0$), for a distance exceeding several Rayleigh lengths, the intensity of the laser field becomes much weaker, and therefore the acceleration becomes inconspicuous. From this discussion, we may conclude that there exists an acceleration channel in the field of a focused laser beam propagating in vacuum, which shows characteristics similar to that of a wave guide tube of conventional accelerators: subluminous phase velocity in conjunction with a strong longitudinal electric field component. Consequently, if one can inject fast electrons into this channel, then some of them may remain synchronous with the accelerating phase for a sufficiently long time such that they receive considerable energy from the field.

4 Results and discussions

In this paper, we assume that the electron bunch is a prolate ellipsoid, which has the same size as the laser pulse, and is injected into the laser field with its central section being in the x–z plane. The electrons in the bunch are assumed to be uniformly distributed in space, with the same initial energy, but a small geometric transverse emittance.

4.1 *Characteristics of the interaction process*

A snapshot describing the interaction process is shown in Fig. 3. It reveals the changes of the electron distribution in space forced by the laser field during the interaction period. Figure 3a describes the initial state of the electrons

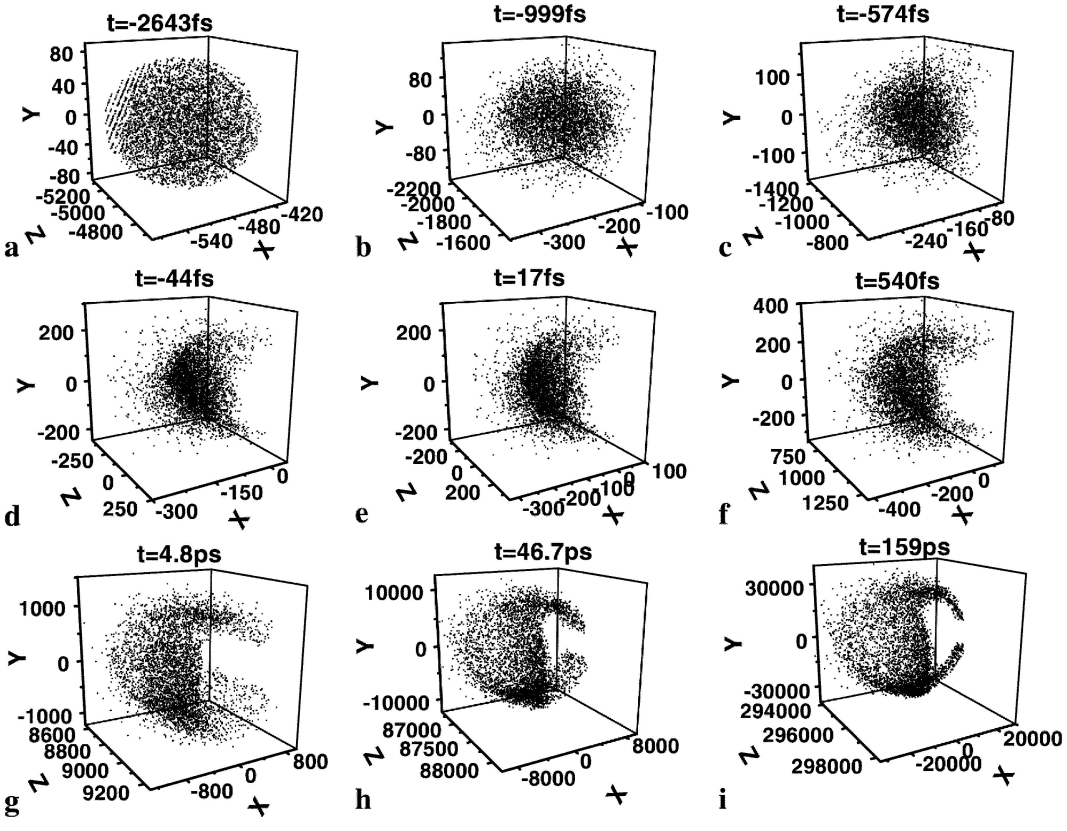

FIGURE 3 Snapshots of an electron bunch scattered by an ultra-intense laser beam. The laser parameters used are $kw_0 = 60$, $\tau = 59$ fs, $\lambda = 1\,\mu$m, $a_0 = 10$ (corresponds to a laser power of $P = 392$ TW and a laser energy of $E \sim 63$ J) and $\theta = \tan^{-1} 0.1$. The incident electron bunch has the same size as the laser pulse with an initial energy, $\gamma_i = 9.6$ (~ 4.9 MeV), for each electron and geometric space emittance of 0.1π mm mrad. We terminate the calculation at $t = 159$ ps, corresponding to $z \sim 5$ cm

uniformly distributed in the ellipsoidal bunch corresponding to $t = -2643$ fs. At $t = -999$ fs (Fig. 3b), the bunch still does not interact with the laser field, and the motions of the electrons are determined by their initial parameters that keep the bunch with an ellipsoidal outline, but enlarged due to the initial emittance. At $t = -574$ fs (Fig. 3c), some electrons in the bunch encounter the front edge of the laser field and are scattered ponderomotively toward the minus-x direction. In the period from $t = -44$ fs to $t = 17$ fs, the center of the laser pulse and that of the electron bunch come together and a large number of electrons interact with the laser field. Some of them are scattered, while others are captured and accelerated. The bunch is "compressed" in the x-direction and the mass center of the bunch reaches its nearest position to the z-axis. After this, it will bounce in the opposite direction. After the intensive interaction period, the states of the electrons are changed. The inelastically scattered (IS) electrons move away at larger scattering angles, while the CAS electrons, which enter the acceleration channels and are accelerated chiefly by the electric axial component of the laser field [5], remain in the field for a long time. This can be seen from the figure of $t = 540$ fs. When the role of the laser field gets weaker ($t = 4.8$ ps) and then totally disappears ($t = 46.7$ ps), a hole appears in the central part of the bunch induced by the scattering and capture effects. The shape of the output bunch stays unchanged with the growing hole until the end of our calculation.

The output electrons can be divided into three groups: the transit electrons, the CAS electrons, and the IS electrons. The transit electrons occupy the region of $x > 0$ and $p_{xf} > 0$ without noticeable acceleration. The IS electrons move without noticeable acceleration and populate the region $x < 0$ and $p_{xf} < 0$; The CAS electrons are greatly accelerated by the laser field ($p_{zf} \gg p_{zi}$ and $p_{xf} \ll p_{zf}$) and are located in the region of $x < 0$.

4.2 *Spatial distribution*

Figure 4 shows the correlation between the final energy of the electrons, γ_f, and their spatial distribution. The output electrons greatly spread in the transverse direction but less in the longitudinal one. This stems from the fact that the longitudinal momenta of the outgoing electrons are very high since the velocities of electrons in the longitudinal direction are almost the same, very close to the speed of light c, while the transverse momenta are very low and the velocities in these directions greatly differ from each other due to the transverse emittance.

4.3 *Energy and angular spectra*

In order to evaluate the quality of the outgoing bunch, we show the electron energy and angular spectra in Fig. 5 (the data were taken from that at $t = 159$ ps and the electron bunch arrives at about $z \approx 5$ cm). The energies of the output electrons are widely spread. The fraction of CAS electrons is about 10% of the total incident electrons. This feature is due to the fact that the incident electrons encounter all phases of

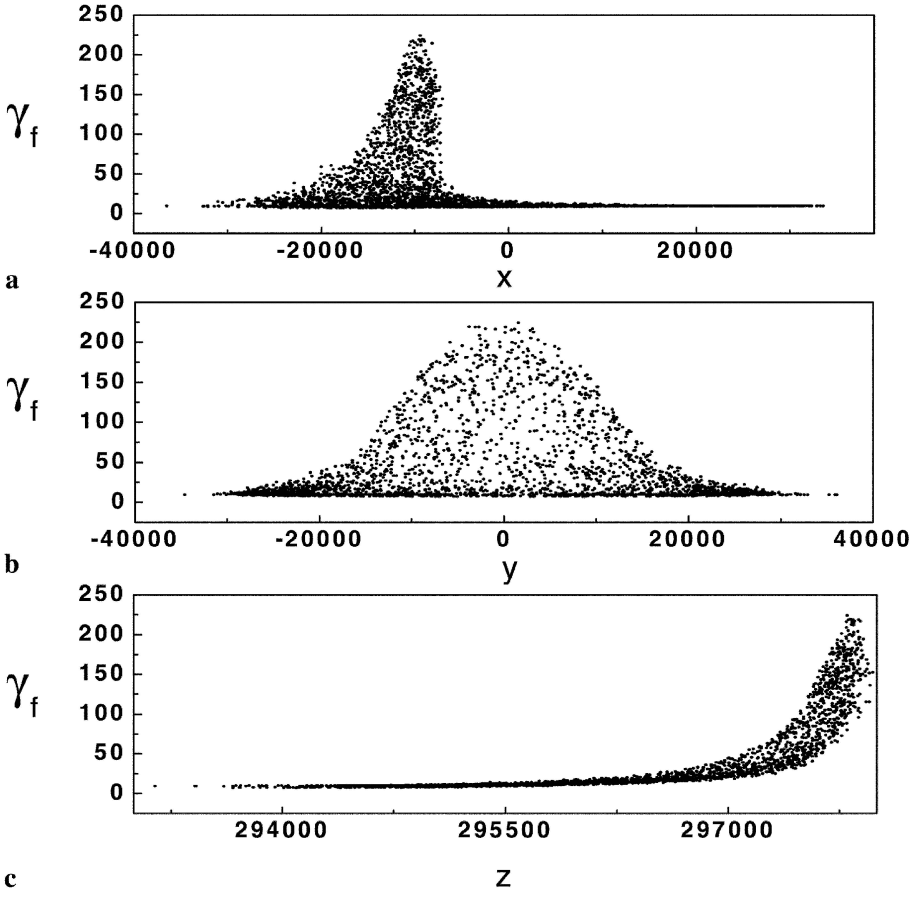

FIGURE 4 Distribution of the energy of the outgoing electrons, γ_f, vs. space coordinates. **a** γ_f vs. kx; **b** γ_f vs. ky; **c** γ_f vs. kz. Parameters used here are the same as those in Fig. 3

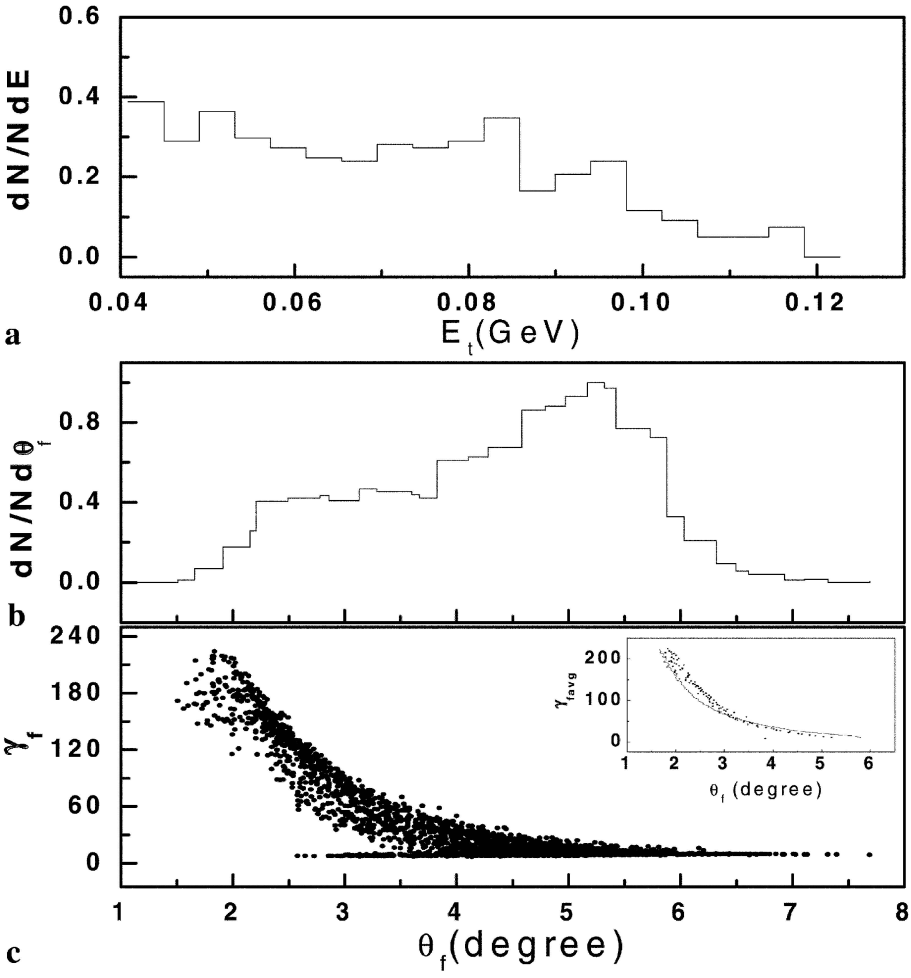

FIGURE 5 Properties of the outgoing electrons (data were taken from that at $t = 159$ ps of Fig. 3). **a** Energy spectrum (In this case, only part of the outgoing electrons which have relatively higher energies are considered). **b** Angular spectrum. **c** Correlation of γ_f vs. θ_f. The *insert* in **c** is a comparison of γ_{fmn} obtained from (19) (*solid line*) and from the simulations (*dots*). γ_{fmn} is the mean final energy of the electrons with the same scattering angle. Parameters used here are the same as those in Fig. 3

each laser period. Thus, some electrons are accelerated by the CAS scheme and others are ponderomotively scattered, depending on the phase when the electron enters the laser field. In principle, the output electron bunch can be run through a magnetic spectrometer to select a near-monoenergetic electron micro-pulse train.

Figure 5b presents the angular distribution $\mathrm{d}N/(N\,\mathrm{d}\theta_f)$ vs. θ_f of the outgoing electrons, where $\theta_f = \tan^{-1}\left(\sqrt{p_x^2 + p_y^2}/p_z^2\right)$ and N is the sum of all incident electrons. The output electrons can be roughly divided into two groups: CAS electrons and inelastically scattered (IS) electrons. This feature becomes more prominent at higher laser intensities, which can be seen clearly in Fig. 7. The IS electrons can also be termed as ponderomotively scattered (PS) electrons. The CAS electrons are greatly accelerated by the laser field and concentrated in a small region of the scattering angles. In contrast to that, the IS electrons are quickly expelled from the intense region of the laser beam and hence experience little energy exchange with the laser field. They correspond to the broad peaks in the region of larger scattering angle.

The correlation between the output energy of each electron and its scattering angle is given in Fig. 5c; the insert is a comparison of the results of the simulations with the theoretical prediction [15]. The figure reveals that the simulation of the energy-angular correlation is roughly consistent with the equation derived from the classical Hamilton–Jacobi theory [15],

$$\theta_f = \tan^{-1}\sqrt{p_{\perp i}^2 + 2(\gamma_i - p_{zi})(\gamma_f - \gamma_i)}/(p_{zi} + \gamma_f - \gamma_i)\,. \quad (19)$$

However, there are obvious deviations. The insert shows that the variation of γ_f with θ_f is closely consistent with (18) for IS electrons, but larger deviations occur for CAS electrons. This might be due to the following reasons: First, the laser field used to derive (19) is a plane wave and the longitudinal component of the EM field is not taken into account. In contrast, in our calculations, we use a Gaussian beam to describe the laser field and the longitudinal component plays a very important role for the CAS case [5]. Second, the relationship between the scattering angle, θ_f, and the final energy, γ_f, given by (19) is one-to-one, while our simulations display a more complicated pattern, as we set a non-zero emittance to the initial state of the electrons in the calculation.

Combining the features of the energy and angular spectra, we can say that the outgoing CAS electrons constitute a high-energy bunch with limited spread in space, while the outgoing IS electrons spread greatly in space with low energies.

4.4 *Emittance*

Experimentally, the root-mean-square (RMS) emittance is used to evaluate the quality of the output bunch.

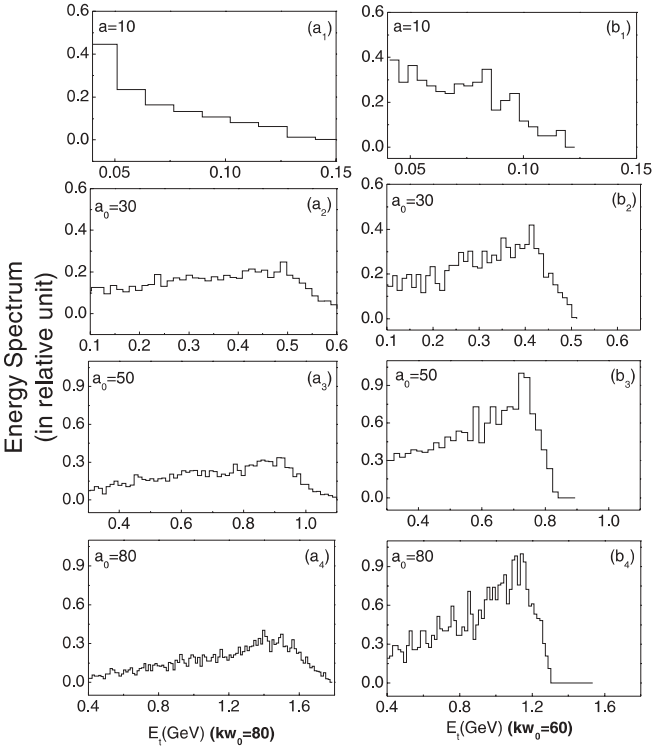

FIGURE 6 Energy spectra of the output electrons at different laser intensities. **a** The spectra on the left are for $kw_0 = 80$, $\gamma_i = 12.101$ (~ 6.2 MeV). **b** The spectra on the right are for $kw_0 = 60$, $\gamma_i = 9.6$ (~ 4.9 MeV). (a_1, b_1), (a_2, b_2), (a_3, b_3), and (a_4, b_4) are for $a_0 = 10$, 30, 50 and 80, respectively. The other parameters used here are the same as those in Fig. 3

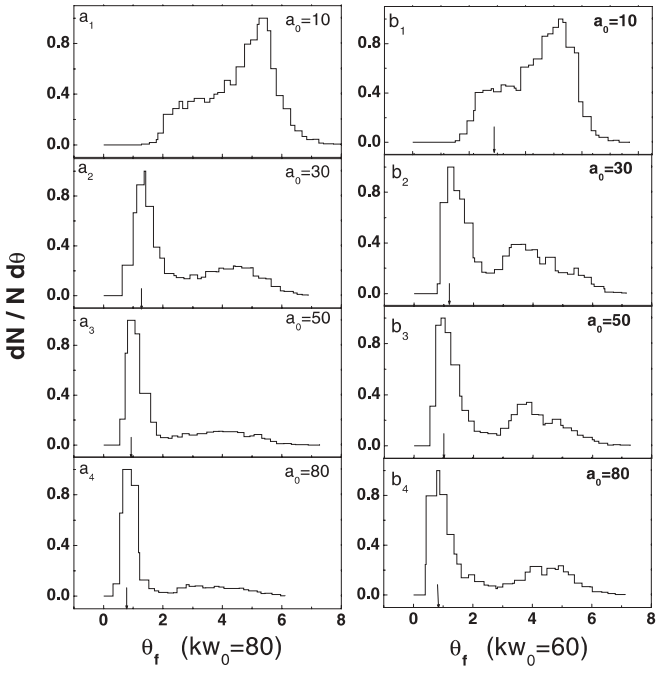

FIGURE 7 Angular spectra of the output electrons at different laser intensities. **a** The spectra on the left are for $kw_0 = 80$, $\gamma_i = 12.101$; **b** The spectra on the right are for $kw_0 = 60$, $\gamma_i = 9.6$. (a_1, b_1), (a_2, b_2), (a_3, b_3), and (a_4, b_4) are for $a_0 = 10$, 30, 50 and 80, respectively. The other parameters used here are the same as those in Fig. 3. The vertical bar shows the scattering angle corresponding to the peak of the CAS electrons

The RMS emittance can be obtained from the following formula [16]

$$\begin{aligned}\epsilon_{x\mathrm{rms}} &= 4\left[\frac{\int \mathrm{d}x \int \mathrm{d}x' \,(x-\langle x\rangle)^2\, g(x,x')}{\int \mathrm{d}x \int \mathrm{d}x' g(x,x')}\right]^{\frac{1}{2}} \\ &\quad\times\left[\frac{\int \mathrm{d}x \int \mathrm{d}x' \left(x'-\langle x'\rangle\right)^2 g(x,x')}{\int \mathrm{d}x \int \mathrm{d}x' g(x,x')}\right]^{\frac{1}{2}}, \\ &= 4\left\langle (x-\langle x\rangle)^2\right\rangle^{\frac{1}{2}} \left\langle (x'-\langle x'\rangle)^2\right\rangle^{\frac{1}{2}}, \\ &= 4\Delta x_{\mathrm{rms}}\Delta x'_{\mathrm{rms}}, \end{aligned} \tag{20}$$

where x is the particle coordinate in transverse direction. The quantity, $x' = p_x/p_z$ is the inclination of the electron trajectory relative to the z-axis, with p_x and p_z being the momenta of electron in the transverse and longitudinal directions, respectively; $g(x, x')$ is the continuous distribution function in the trajectory space, Δx_{rms} is the RMS width of the bunch, and $\Delta x'_{\mathrm{rms}}$ is the RMS angular width.

Calculations of electron emittances in specific energy ranges are shown in Table 1. It is of interest to note that, compared with the incident value, the emittances of the output electrons in the x-direction are diminished, whereas in the y-direction they are of the same order of magnitude. The reason for this is as follows. Since the laser field is x-polarized in the x-direction, the CAS electrons are bent in a small region whereby p_x changes much less than p_z. This effect causes the range of variation of coordinates and angles in the x-direction to decrease, thereby diminishing ϵ_x. In the y-direction, the decrease in p_y/p_z is compensated by the increase in the range of coordinate space; thus ϵ_y is of the same magnitude as its initial value.

Notice that the acceleration is chiefly in the longitudinal direction. The force experienced by the electrons in the y-direction is extremely small compared with the force in the x- and z-directions. These features are consistent with the basic theory of conventional linacs [16].

4.5 *Influence of laser parameters on the output properties*

In our previous studies [5], we found that there are many factors that affect the efficiency of the CAS scheme, such as laser intensity, beam width, pulse duration, electron initial energy, electron incident angle, etc. In this paper, we concentrate our studies on the effects of the laser parameters intensity, beam width, and pulse duration on the properties of the output electrons.

4.5.1 Laser intensity. The energy and angular spectra of the output electrons at different laser intensities are shown in Figs. 6 and 7, respectively. These figures unveil the following features. The energies of the CAS electrons spread widely due to the same reason as mentioned above concerning Fig. 5. In Fig. 6 (Fig. 7) a peak emerges at $a_0 = 30(10)$, for $kw_0 = 80(60)$ in the higher energy part of the spectrum; it becomes more prominent with increasing laser intensity. This means that not only the energy of the output CAS electrons will

a_0	10	30	50	80
Maximum output energy (MeV)	114.5	491.4	814.1	1281
Fraction of CAS electrons (%)	10.4%	34.0%	44.1%	48.0%
Mean scattering angle $\bar{\theta}_f$	...	0.9°	1.1°	1.4°
RMS deviation of the scattering angles ($\Delta\bar{\theta}_f$)	...	±0.1°	±0.2°	±0.3°
Emittance of the outgoing electrons $\in_i$ (π mm mrad)	$\in_{1x}=0.016$ $\in_{1y}=0.52$ $\in_{2x}=0.008$ $\in_{2y}=0.31$ $\in_{3x}=0.029$ $\in_{3y}=0.48$ $\in_{4x}=0.058$ $\in_{4y}=0.83$	$\in_{1x}=0.054$ $\in_{1y}=0.49$ $\in_{2x}=0.02$ $\in_{2y}=0.31$ $\in_{3x}=0.045$ $\in_{3y}=0.52$ $\in_{4x}=0.054$ $\in_{4y}=0.60$	$\in_{1x}=0.037$ $\in_{1y}=0.29$ $\in_{2x}=0.035$ $\in_{2y}=0.28$ $\in_{3x}=0.065$ $\in_{3y}=0.43$ $\in_{4x}=0.067$ $\in_{4y}=0.44$	$\in_{1x}=0.037$ $\in_{1y}=0.32$ $\in_{2x}=0.058$ $\in_{2y}=0.29$ $\in_{3x}=0.084$ $\in_{3y}=0.37$ $\in_{4x}=0.086$ $\in_{4y}=0.40$

TABLE 1 Some important data of the outgoing electrons at different laser intensity. Here, CAS electrons refer to those electrons with final energies, $\gamma_f > \frac{1}{2}\gamma_{fm}$. The $\in_i$ represent the emittances of the near-monoenergetic CAS electron micropulse trains with final energies in the range $\gamma_{fi} \pm \Delta\gamma_{fi}$, where $\gamma_{f1} = 0.5\,\gamma_{fm}$, $\gamma_{f2} = \gamma_{f3} = \gamma_{f4} = 0.8\,\gamma_{fm}$, $\Delta\gamma_{f1} = 2\%\gamma_{f1}$, $\Delta\gamma_{f2} = 2\%\gamma_{f2}$, $\Delta\gamma_{f3} = 8\%\gamma_{f3}$, and $\Delta\gamma_{f4} = 15\%\gamma_{f4}$. Laser beam width $kw_0 = 60$

increase with laser intensity, but also the fraction of CAS electrons out of the total electrons will increase. This feature will be useful for tailoring the output electron beam (see Fig. 6). The non-CAS electron peak is especially prominent in Fig. 7 (a_1, b_1) because at a laser intensity of $a_0 = 10$, the IS and transmitted electrons are more than 80% of the incident electrons; accordingly, the peak of the CAS electrons becomes inconspicuous. As we know, there exists an intensity threshold, a_0^T; only when $a_0 > a_0^T$, the CAS will work [16, 17]. With increasing laser intensity, the region above the laser intensity threshold where the CAS scheme works is enlarged. This causes the fraction of CAS electrons to increase, and leads to a more prominent CAS peak. The CAS peak moves toward small scattering angles with increasing laser intensity, as indicated by the vertical bars in Fig. 7. This feature is consistent with (19).

Table 1 gives some important data for the outgoing electrons at different laser intensities. The results illustrate that the energy gain of the output electrons is found to increase approximately linearly with a_0 for $10 \le a_0 < 100$, which is consistent with our theoretical result, $\gamma_{fm} = \frac{\arctan(b)}{e} a_0 k w_0$, where b is a constant [18]; substantial energy gains > 100 MeV can be obtained for currently existing laser systems of ≈ 100 TW power. This feature is in agreement with theoretical estimates based on acceleration in the axial laser field. For CAS electrons in a near monoenergetic region with $\gamma_f \sim 900 \sim 1000$, the mean scattering angle, $\bar{\theta}_f$, and the RMS deviation of the scattering angle, $\Delta\bar{\theta}_f$, are slightly dependent on the laser intensities. The physical explanations for these features are the same as those for Fig. 5c.

The emittances of the near-monoenergetic CAS electron micro-pulse trains at different laser intensities are also shown in Table 1.

From the above discussion, we conclude that with increasing laser intensity, the final energy gain, the fraction of CAS electrons, and the energy dispersion of the outgoing CAS electrons are improved.

4.5.2 Laser beam width. What will happen to the output electrons if the laser beam width changes at constant laser intensity? This will be answered in the following.

Figure 8 and Table 2 show the variations of the maximum output energy, γ_{fm}, and the fractions of CAS electrons, n/N, where n is the number of CAS electrons, in the whole bunch vs. laser beam width kw_0. Four beam widths, $kw_0 = 40$, 60, 80, and 100, are chosen. For each beam width, the best incident momentum is selected. Here, "best" means that with this parameter the efficiency of CAS electrons obtained is maximized [17]. The results show that with decreasing w_0, the fraction of CAS electrons increases. On the other hand, the maximum energy increases linearly with w_0.

These characteristics can be understood as follows. First, the laser intensity threshold $(a_0)_{th}$ for the CAS electron to emerge is critically dependent on the beam width, w_0, as $(a_0)_{th} = \frac{\gamma_f^T}{\int_0^{t_\Delta} \frac{2}{ew_0(1+\alpha^2)} \cos[\varphi+\varphi_0]\,dt}$, in which $\gamma_f^T = \frac{kw_0}{\sqrt{2-1/(kw_0)^2}}$, and t_Δ is the time when the electron is driven to the phase velocity, v_φ, along the electron trajectory [18]. Thus, with increasing w_0, the intensity threshold $(a_0)_{th}$ also increases. So the number of electrons in the above-threshold region will

kw_0	40	60	80	100
Maximum output energy (MeV)	89.1	114.5	130.3	149.6
Fraction of CAS electrons (%)	10.6%	10.4%	6.4%	2%
Emittance of the output electrons (π mm mrad)	$\in_x=0.053$ $\in_y=0.90$	$\in_x=0.058$ $\in_y=0.826$	$\in_x=0.046$ $\in_y=0.37$	$\in_x=0.031$ $\in_y=0.135$

TABLE 2 Some important data of the outgoing electrons at different laser beam widths at $a_0 = 10$. Other parameters used are the same as there in Fig. 8. The $\in$ represent the emittances of the near-monoenergetic CAS electron micropulse trains with final energies in the range $\gamma_f \pm \Delta\gamma_f$, where $\gamma_f = 0.8\,\gamma_{fm}$, $\Delta\gamma_f = 15\%\gamma_f$

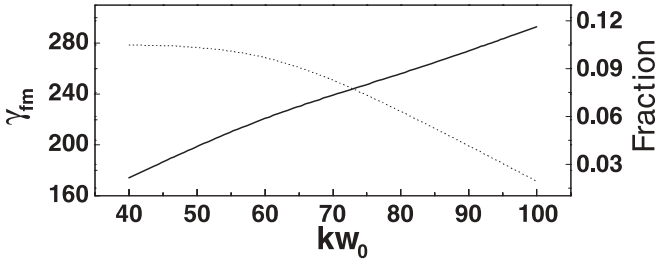

FIGURE 8 Dependence of the maximum output energy, $\gamma_{\rm fm}$, (*solid line*) and the fraction of the CAS electrons (*dotted line*) on the beam width kw_0. The electron incident energy is taken to be the optimum value for each w_0, that is $\gamma_{\rm i} = 8.6$ for $kw_0 = 40$, $\gamma_{\rm i} = 9.05996$ for $kw_0 = 60$, $\gamma_{\rm i} = 12.101$ for $kw_0 = 80$, and $\gamma_{\rm i} = 17.6157$ for $kw_0 = 100$. The other parameters used here are the same as those in Fig. 3

decrease, leading to lower CAS efficiency. Second, the work ΔW done by the laser field on the electron in the longitudinal direction is proportional to the beam width w_0. This can be seen from the following arguments. One has $\Delta W = E_z z$, where $E_z \propto E_x \frac{1}{kw_0}$, and $z \sim z_{\rm R} = \frac{kw_0^2}{2}$, thus $\Delta W \propto w_0$. Therefore, with increasing w_0, the maximum energy, $\gamma_{\rm f\,max}$, of the electron gained from the laser field also increases.

Table 2 gives the emittances of electron trains at a specific energy range for different beam widths, w_0. For smaller beam widths, w_0, the diffraction effect becomes more prominent, leading to more electrons scattered by the edge of the laser field, thus increasing the emittance.

4.5.3 Laser pulse duration. From (3) and (6), it can be seen that the laser pulse duration, τ, has less influence on the electromagnetic components of the laser field in the present long-pulse approximation. Therefore, the effects of pulse duration on the properties of the output electrons are inconspicuous. The results presented in Table 3 also show the same features.

It is worthy to mention that in the above calculations and simulations all input electrons have the same initial energy. This assumption is far from realistic experimental conditions. However, from our studies [17] we found that there exists a momentum region of the incident electrons for CAS to occur. It means that the fractions and energy spectra of the CAS electrons are not very sensitive to the exact value of the electron incident energy. Thus an electron bunch with some energy spread is tolerable. Hence for proof-of-principle experiments, the electron bunches may stem from intense laser-gas jet interactions and need not to be produced in electron accelerators.

τ (fs)	159	265	371
Maximum output energy (MeV)	114.5	111.7	116.8
Fraction of CAS electrons (%)	10.4%	8.9%	9.5%
Emittance of the output electrons ($\pi \cdot$mm$\cdot$mrad)	$in_x = 0.058$ $in_y = 0.826$	$in_x = 0.072$ $in_y = 0.78$	$in_x = 0.068$ $in_y = 0.80$

TABLE 3 Some important data of the outgoing electrons at different laser beam pulse duration at $a_0 = 10$. Other parameters used are the same as there in Fig. 2. The $\in$'s are the same as there in Table 2

5 Conclusion

We studied the characteristics of electrons accelerated by the CAS. The results can be summarized as follows. (i) The outgoing electrons can be divided into two groups: CAS electrons, which have high energies and small scattering angles (less than 3^0) with respect to the laser beam and IS electrons, which have low energies and spread widely in space. (ii) The output electrons disperse largely in the transverse direction, with limited spread in the longitudinal direction. (iii) The emittance of the output electron trains in the polarization direction of linearly polarized laser field is improved after the interaction, while that in the other transverse direction stays about the same. (iv) The energy gain is found to increase linearly with a_0 for $10 \le a_0 < 100$ and substantial energy gains (> 100 MeV) can be obtained from today's laser systems (≈ 100 TW). (v) For nearly mono-energetic CAS electrons, the scattering angle changes with the laser intensity only slightly. This feature can help to extract electron micropulse trains with a required energy by using a spectrometer. (vi) With increasing laser intensity, the final energy gain, the fraction of CAS electrons, the energy dispersion, and the emittance of the outgoing CAS electrons are improved. (vii) At the same laser intensity, the CAS fraction increases with decreasing beam width, while the maximum output energy increases with increasing beam width. (viii) The laser pulse duration has little influence on the properties of the output electrons in the long-pulse approximation.

The above results indicate that CAS is a promising scheme for vacuum laser accelerators.

ACKNOWLEDGEMENTS The authors would like to thank E.H. Esarey for enlightened discussions. This work is supported partly by the National Natural Science Foundation of China under contracts No.10335030 and 10076002, the National High-Tech ICP Committee in China, the Engineering-Physics Research Institute Foundation of China, and the National Key Basic Research Special Foundation (NKBRSF) under Grant No.1999075200.

REFERENCES

1 A.M. Sessler: Am. J. Phys **54**, 505 (1986)
2 M.D. Perry, G.A. Mourou: Science **264**, 917 (1994); E. Esarey, P. Sprangle, J. Krall, A. Ting: IEEE Trans Plasma Sci **24**, 252 (1996); B. Quesnel, P. Mora: Phys. Rev. E **58**, 371 (1998); A. Pukhov, J. Meyer-Ter-Vehn: Appl. Phys. B **74**, 355 (2002); A. Pukhov: Rep. Prog. Phys. **66**, 47 (2003); V. Malka, et al.: Science **298**, 1596 (2002)
3 G. Malka, E. Lefebvre, J.L. Miquel: Phys. Rev. Lett. **78**, 3314 (1997); K.T. McDonald: Phys. Rev. Lett. **80**, 1350 (1998); P. Mora, B. Quesnel: Phys. Rev. Lett. **80**, 1351 (1998); E. Lefebvre, et al.: Phys. Rev. Lett. **80**, 1352 (1998)
4 P.H. Bucksbaum, M. Bashkansky, T.J. Mcllrath: Phys. Rev. Lett. **58**, 349 (1987); F.V. Hartemann, E.C. Landahl, A.L. Troha, Jr,J.R. Van Meter, H.A. Baldis, R.R. Freeman, N.C. Luhmann, Jr., L. Song, A.K. Kerman, D.U.L. Yu: Phys. Plasmas **6**, 4104 (1999); G.V. Stupakov, M.S. Zolotorev: Phys. Rev. Lett. **86**, 5274 (2001)
5 J. Pang, Y.K. Ho, X.Q. Yuan, N. Cao, Q. Kong, P.X. Wang, L. Shao, A.M. Sessler, E. Esarey: Phys. Rev. E **66**, 066 501 (2002); P.X. Wang, Y.K. Ho, X.Q. Yuan, Q. Kong, N. Cao, A.M. Sessler, E. Esarey, Y. Nishida: Appl. Phys. Lett. **78**, 2253 (2001)
6 P.M. Woodward: J. IEEE **93**, 1554 (1947); J.D. Lawson: IEEE Tran. Nucl. Sci. NS-**26**, 4217 (1979); E. Esarey, P. Sprangle, K. Krall: Phys. Rev. E **52**, 5443 (1995); P. Sprangle, E. Esarey, K. Krall: Phys. Plasmas **3**, 2183 (1996)

7 Y.C. Huang, R.L. Byer: Appl. Phys. Lett. **69**, 2175 (1996); R.L. Byer, T. Pletter, C. Barnes; E. Colby, B. Cowan, R.H. Siermann, J.E. Spencer: Proc. 2001, Particle Accel. Conf. (in press)
8 M.V. Fedorov, S.P. Goreslavsky, V.S. Letokhov: Phys. Rev. E **55**, 1015 (1997)
9 C.S. Chen: Phys. D **17**, 434 (1978)
10 P.W. Milonni, J.H. Eberly: *Lasers* (Wiley, New York 1998)
11 E. Esarey, P. Sprangle, M. Pilloff, J. Krall: J. Opt. Soc. Am. B Vol **12**(9), 1695 (1995)
12 M. Lax: Phys. Rev. A **11**, 1365 (1975); L.W. Davis: ibid. **19**, 1177 (1979)
13 J. Barton, D.R. Alexander: J. Appl. Phys. **66**, 2800 (1989)
14 N. Cao, Y.K. Ho, P.X. Wang, Q. Kong, X.Q. Yuan: Opt. Commun. **204**, 7 (2002)
15 Y.I. Salamin, F.H.M. Faisal: Phys.Rev. A **55**, 3678 (1997); F.V. Hartemann, J.R.V. Meter, A.L. Troha, et al: Phys. Rev. E **58**, 5001 (1998)
16 S. Humphries, Jr: *Charge Particle Beams* (John Wiley & Sons, Inc. 1990)
17 Q. Kong, Y.K. Ho, N. Cao, J. Pang, P.X. Wang, L. Shao: Appl. Phys. B **74**, 517 (2002)
18 J. Pang, Y.K. Ho, N. Cao, Y.J. Xie, L. Shao, Z. Chen, S.Y. Zhang: Appl. Phys. B **76**, 617 (2003)